

COMPARISON OF TES FFSM EDDIES AND MOC STORMS, MY 24–26

J. Noble, *San Jose State University, NASA Ames Research Center, Mountain View, CA, USA* (*jn2@met.sjsu.edu*), **R. J. Wilson**, *Geophysical Fluid Dynamics Laboratory, NOAA, USA*, **R. M. Haberle**, **J. L. Hollingsworth**, **M. A. Kahre**, *NASA Ames Research Center, Mountain View, CA, USA*, **J. R. Barnes**, *Oregon State University, USA*, **A. F. C. Bridger**, *San Jose State University, NASA Ames Research Center, USA*, **B. A. Cantor**, *Malin Space Science Systems, USA*.

Introduction:

Mars Global Surveyor (MGS) orbiter observed a planet-encircling dust storm (PDS) in Mars year (MY) 25 from $L_s=176.2$ – 263.4° . Although PDSs occur on an irregular basis, all well-documented storms have begun within $\pm 75^\circ$ of L_s from perihelion ($L_s=251^\circ$) when insolation is greatest near the SH summer solstice ($L_s=270^\circ$) and the south polar cap is receding. PDS seasonal occurrence suggests the presence of climatic/environmental precursors and components, yet interannual variability suggests that initiation and expansion mechanisms are not solely seasonal in character (Zurek and Martin 1993).

We have integrated and examined all available MGS data in order to better understand and characterize the dynamical processes responsible for MY 25 PDS initiation and expansion (Haberle *et al.* 2005; Noble *et al.* 2006). Here we present an examination of Mars Orbiter Camera (MOC) dust storms and transient baroclinic eddies identified from Fast Fourier Synoptic Mapping (FFSM) of Thermal Emission Spectrometer (TES) temperatures for the first two phases of the storm: precursor, $L_s=176.2$ – 184.7° , and expansion, $L_s=184.7$ – 193° .

FFSM analysis of TES 3.7 hPa thermal data shows the presence of eastward-traveling waves at 60° S with a period of about three sols. We hypothesize that these waves are transient baroclinic eddies that contributed to the initiation of precursor storms near Hellas.

Datasets: FFSM is a spectral analysis method that creates synoptic maps from asynoptic data, maintaining full space-time resolution without distorting or smoothing higher frequency (~ 1 – 3 sols) weather signals (Barnes 2001, 2003, 2006). This process removes the time mean, zonal mean, and westward diurnal tide. Figures 2–4 are longitude-time plots of TES 3.7 hPa temperature anomalies at 60° S for MY 24–26. Figures 2 and 3 compare eddies and dust storms from $L_s=165$ – 188° during MY 24 and 25 respectively. Arrows delimit the longitudinal extent of dust storms based on our analysis of MOC images provided by Cantor (2007). Three arrow sizes represent a subjective magnitude scale of apparent convective activity/structure, while colors represent storm central latitudes: black ($< 45^\circ$ S), grey (35 – 45° S), and white (25 – 35° S). FFSM data

have 5° longitudinal resolution, while storm arrows have 1° .

FFSM eddies MY 24–26: SH eddy amplitudes are greatest at $\sim 60^\circ$ S, and diminish significantly south of 65° S and north of 40° S. Eddy structure and amplitude also change with height. For example, strong cold anomalies are predominant in Hellas at 60° S from $L_s=174$ – 180° at 3.7–1.36 hPa. By 0.5 hPa, strong warm anomalies emerge that amplify with height, dominating the field at 0.1 hPa.

Globally coherent eddies maintain amplitude throughout all or most longitudes. While coherency in the full eddy field (all wavenumbers) appears to be disrupted by SH orography, particularly Argyre and Hellas, wavenumber 3 eddies do not show such disruption.

MY24: Coherent, strong-amplitude cold anomalies are present in the 150 – 330° E storm zone for the entire time domain (Fig. 2). Eddy activity within the storm zone appears to shift eastward in time, with strongest eddies appearing in the ~ 130 – 240° E sector from $L_s=165$ – 173° , and in the ~ 230 – 330° E sector from $L_s=175$ – 187° . Their apparent weakening from 330 – 120° E suggests orographic disruption from Argyre and Hellas, as simulated by Hollingsworth (2005). Few strong-amplitude eddies (cold anomalies) maintain amplitude and coherency east of 30° E, the most notable persists until 120° E at $L_s=183.7^\circ$.

Major cap-edge storms south of Hellas occur less frequently in MY 24 MOC images compared to MY 25. The most prominent are described below. At $L_s=169.9^\circ$ large cap-edge storms occurred east of Argyre at 345° E and within Hellas at 80° E. Six sols later at $L_s=173.3^\circ$ a large storm emerged west of Hellas, followed by a smaller one in SW Hellas three sols later at $L_s=175.1^\circ$. At $L_s=180.2^\circ$ a large cap-edge storm developed between Argyre and Hellas (~ 330 – 25° E), along with a storm in NW Hellas. The latter storm appears to stay confined to northern Hellas and grows for the next three to four sols, visibly diminishing by $L_s=182^\circ$.

MY25: Coherent, strong-amplitude cold anomalies are present in the 150 – 330° E storm zone for most of the time domain, and their centers appear to shift slightly eastward over time (Fig. 3). Eddies 1–6 have a ~ 3 sol period at 240° E. This general pattern is similar to MY 24. An outstanding difference be-

tween the two years is the degree to which strong-amplitude eddies persist through Noachis and extend (undiminished) into Hellas. This occurs throughout the precursor phase from $L_s=174-180^\circ$. The cold anomaly passing through Hellas between $\sim L_s=176-179^\circ$ appears to be among the largest temporally, spatially, and amplitudinally during the precursor phase. The corresponding cap-edge storm at $L_s=177.5^\circ$ appears to have the most intense convective activity of this phase (Fig. 5b).

MY 26: Figure 4 shows MY 26 eddies for $L_s=175.39-192.79^\circ$. This time range was chosen due to missing data from $L_s=165-175^\circ$. MY 26 data show a different seasonal regime compared with MY 24 and 25. Although some coherent transient eddies are visible in the storm zone described above, a strong stationary wave is visible. Cold centers appear to dominate the $\sim 90-220^\circ$ E longitude corridor from $L_s=175-183^\circ$, followed by a polarity switch to warm centers from $L_s=183-192^\circ$.

Interannual eddy variability MY 24–26: The data show moderate interannual variability of eddy activity in MY 24 and 25, and significant variability when comparing MY 26 with MY 24 and 25. In MY 24 and 25, maximum amplitude cold centers appear predominantly in the storm zone from $120-330^\circ$ E. MY 25 eddies 1–3, however, are relatively high-amplitude in Hellas and low in Tharsis. Figure 1 shows MY 24–26 FFSM cold anomaly amplitudes vs. time in Hellas ($45-90^\circ$ E, $50-60^\circ$ S). MY 25 eddies during the precursor phase are moderately stronger amplitude than corresponding MY 24 eddies, and significantly stronger than those in MY 26.

Phase and Periodicity: Phase speed was calculated with

$$c(x)=\Delta x/\Delta t,$$

where $\Delta x = (r_{eq} \cdot \cos\varphi) \cdot \Delta\lambda$, r_{eq} is planetary radius, φ latitude, λ longitude, and t time at 180° E. MY 24–26 mean global phase speeds of 14.3, 13.8, 13.7 m s^{-1} respectively (Table 1) show that MY 25 eddies were $\sim 0.5 \text{ m s}^{-1}$ slower than those in MY 24. Mean eddy periodicity, P , in Hellas (60° E) was 2.7, 2.9, and 3.1 sols for MY 24–26 respectively (Table 1). Fast Fourier Transform (FFT) power spectra for MY 24–25 Hellas ($40-100^\circ$ E, 60° S) eddies from $L_s=165-188^\circ$ show a dominant periodicity of ~ 3.5 sols for both years and values, along with moderately high adjacent amplitudes at ~ 2.8 sols (Fig. 6). Since there are 80 time steps (40 sols), wave 13 is 6.2 sols, and wave 14 is 5.7. The wide, moderate-amplitude (± 0.5 K) spread from 2.5–4 sols is due to wavenumber resolution and heterogeneous data. FFT power spectra of negative values at ~ 3.5 sols show approximately twice the amplitude in MY 25 compared with MY 24. A comparison of cold anomalies in Hellas show that all eddies (E1–E7) in MY 25 are ~ -3.5 K or colder, compared to two (E5 and E7) in MY 24 (E1 is close at ~ -3.2 K) (Fig. 1).

Transient eddies and storm genesis: FFSM analysis of TES MY 25 temperatures (Barnes 2006) show that seven cold centers (E1–E7) originated in the Tharsis hemisphere and then propagated through Hellas \sim four sols later from $\sim L_s=174-187^\circ$, assuming that they are coherent (or nearly so) from $200-90^\circ$ E (Fig. 3). The first eddy (E1) originated near 230° E at $L_s=173.52^\circ$ and propagated through Hellas from $\sim L_s=175-177^\circ$, corresponding to the first pulse of storm activity described by Cantor (2007). Analysis of MOC storms and FFSM eddies shows that the seven pulses of storm activity identified by Cantor (2007) occur in the time span of the first six eddies (Fig. 3).

Integration of FFSM and MOC MY 24 and 25 data shows interesting temporal and spatial associations between the evolution of eddies and storms, including: 1) comparable periodicities of travelling waves and pulses of storm activity; 2) concurrent eastward propagation of both eddies and storms; and 3) location of high-latitude storms on the leading (eastern) of eddies. These results suggest a causal relationship between baroclinic eddies and local storm initiation.

The three panels in Figure 5 show storms emerging on or near the leading edges of strong-amplitude cold centers during the MY 25 precursor phase. Figures 2 and 3 show a spatial and temporal correlation between eastward eddy propagation and eastward storm evolution. This relationship is visible in MY 24 storm sequences (Fig. 2) starting at $L_s=169.9^\circ$ (330 and 60° E), $L_s=172.7^\circ$ (0° E), and $L_s=184.57^\circ$ (290° E), and also in most MY 25 sequences (Fig. 3), especially as eddies 1, 2, 3, 5, and 6 propagate through Hellas. A northward storm evolution is visible as eddies 2 and 5 pass through Hellas at $\sim L_s=178$ and 182° during MY 25.

Although a first order approximation would locate cold fronts between cold and warm FFSM anomalies, their location can not be determined from FFSM eddies alone – pressure and wind data are also required. The limited longitudinal resolution of TES data, and subsequent 5° longitudinal resolution of FFSM eddy bins, preclude precise determination of cold fronts. Fronts are most intense close to the surface, however TES averaging of the lowest scale height reduces their signal. Furthermore, there is probably a phase shift between FFSM eddy and pressure fields, since isobaric and isosteric surfaces intersect under baroclinic conditions. The nature of Martian baroclinic waves and frontogenesis is understudied and consequently fronts have not been sufficiently investigated. There is a need to better characterize the relationship between cold fronts and surface stress, as well as the role orography plays in disrupting SH transient eddies.

It is important to note that the stronger cold centers in Hellas during the MY 25 precursor phase could be associated with regional cap edge circula-

tions that are not propagating eastward. If they vary in time, they may show up in FFSM transient eddy fields. Stronger cap edge circulations in MY 25 could be due to a strengthening of the Hellas vortex at low levels during this season (Barnes 2010).

Conclusions: An examination of the spatial and temporal relationship of FFSM eddies and MOC storms suggests an interesting association between eastward eddy propagation and eastward storm evolution. We hypothesize that baroclinic eddies played a significant role in triggering the MY 25 precursor phase regional storms. Determining the factors responsible for PDS genesis in MY 25 and not 24 and 26 is difficult. MY 24–26 Hellas periodicities of 2.7, 2.9, and 3.1 sols respectively show minor interannual variability, as well as global phase speeds of 14.3, 13.8, and 13.7 m s⁻¹. The most notable difference is the amplitude of E1–E7 eddies in Hellas (Fig. 1), with all seven MY 25 eddies colder than ~-3.5 K, compared with two (or three) in MY 24 and one (or two) in MY 26. It is possible that the sustained series of high-amplitude eddies in MY 25 was a factor in PDS interannual variability. If other interannual differences in transient eddy activity were involved in MY 25 PDS genesis, then they may be features undetectable by TES, such as very shallow disturbances (Barnes 2010). Non-dynamical factors possibly governing PDS interannual variability include dust sources and sinks.

Constructive interference of transient eddies and other circulation components in MY 25, including sublimation flow, anabatic winds (daytime upslope), diurnal tides, and dust-induced thermal tides, may have led to the initiation, amplification, and sustained expansion of precursory storms. Constructive interference increases surface stresses capable of lifting dust. Dust suspended during the precursor phase greatly amplified thermal tides, that in turn contributed to greater storm growth within, and expansion out of Hellas, compared to other years.

Both the lack and resolution of meteorological data limits the depth of analysis and precludes drawing firm conclusions about storm initiation, expansion, and interannual differences. It is not possible to assess the influence of various circulation components on MY 25 PDS genesis with the available MGS data. We plan to conduct MGCM simulations to decompose such components and assess their contributions to storm initiation and expansion.

References:

- Barnes, J., 1981: Midlatitude Disturbances in the Martian Atmosphere: A Second Mars Year. *Journal of the Atmospheric Sciences*, **38**, 225-234.
- Barnes, J. R., 2001: Asynoptic fourier transform analyses of MGS TES data: Transient baroclinic eddies. *Bulletin of the American Astronomical Society*, **33**, 1088.
- Barnes, J. R., 2003: Mars Weather Systems and Maps: FFSM Analyses of MGS TES Temperature Data. *Sixth International Conference on Mars*,

Pasadena, California, USA.

- Barnes, J. R., 2006: FFSM Studies of Transient Eddies in the MGS TES Temperature Data. *Mars Atmosphere Modelling and Observations*, Granada, Spain.
- Barnes, J. R., 2010: Personal Communication.
- Cantor, B., 2007: MOC observations of the 2001 Mars planet-encircling dust storm. *Icarus*, **186**, 60-96.
- Haberle, R., J. Noble, J. Murphy, A. F. C. Bridger, J. Hollingsworth, J. R. Barnes, B. Cantor, M. C. Malin, and M. Smith, 2005: Synthesis of MGS Observations of the 2001 Global Dust Storm on Mars: Implications for Atmospheric Dynamics. *American Geophysical Union*, San Francisco, CA, USA.
- Hinson, D., and R. Wilson, 2002: Transient eddies in the southern hemisphere of Mars. *Geophysical Research Letters*, **29**.
- Hollingsworth, J. L., 2005: Large-Scale Weather Systems in Mars' Southern Hemisphere: Effects of the Great Impact Basins. *American Geophysical Union, Fall Meeting*, San Francisco, CA, USA.
- Noble, J., R. Haberle, A. Bridger, J. Murphy, J. L. Hollingsworth, J. Barnes, B. Cantor, M. Malin, and M. Smith, 2006: Synthesis of MGS observations of the 2001 global dust storm on Mars. *Mars Atmosphere Modelling*, Granada, Spain.
- Zurek, R. W., and L. J. Martin, 1993: Interannual variability of planet-encircling dust storms on Mars. *Journal of Geophysical Research*, **98**, 3247-3259.

Table 1: Baroclinic eddy (global) phase speeds, c (m s⁻¹), and period, P (sols), at 60° E, MY 24–26

~L _s (°) eddy at 60° E	Eddy #	c MY24	c MY25	c MY26	P MY24	P MY25	P MY26
176.5	E1	12.8	13.8				
178.0	E2	13.4	14.5	15.6	2.7	2.8	
179.3	E3	14.1	14.8	14.3	2.6	2.5	2.8
181.0	E4	14.5	13.1	13.8	2.8	3.0	2.9
182.7	E5	15.2	13.5		2.7	2.9	
184.6	E6	16.0	13.8	12.9	2.5	2.8	
186.3	E7	13.8	13.2	11.8	2.9	3.3	3.7
	Mean	14.3	13.8	13.7	2.7	2.9	3.1

Figures:

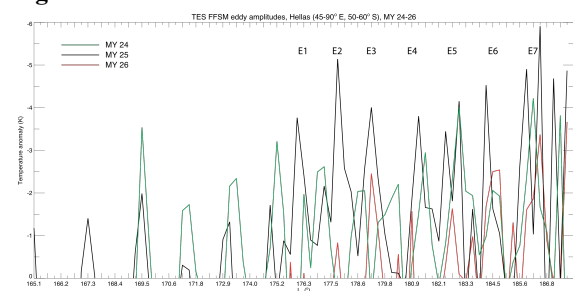


Figure 1: Evolution of TES FFSM eddy amplitudes in Hellas (45–90° E, 50–60° S) for MY 24–26

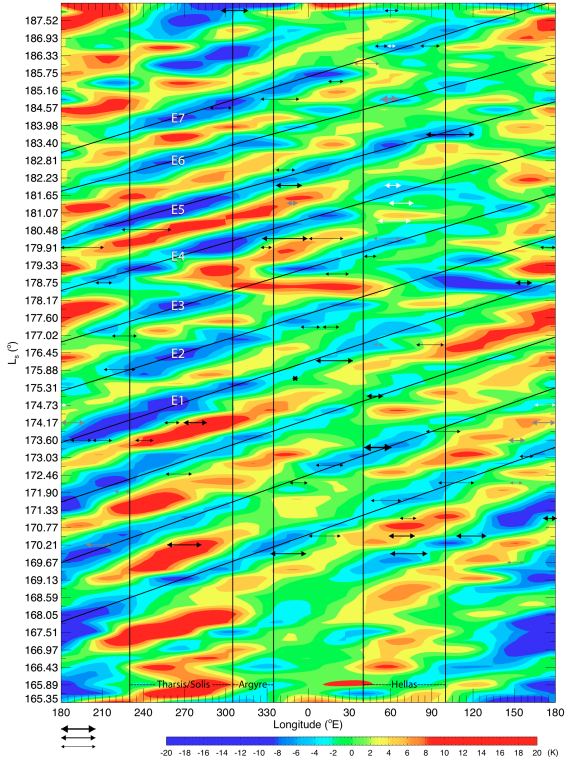


Figure 2: TES 3.7 hPa FFSM eddies at 60° S and MOC storms, MY 24. Arrows delimit longitudinal extent of MOC storms. Three arrow sizes represent a subjective magnitude scale of apparent convective activity/structure. Colors represent storm central latitudes: black (< 45° S), grey (35–45° S), and white (25–35° S).

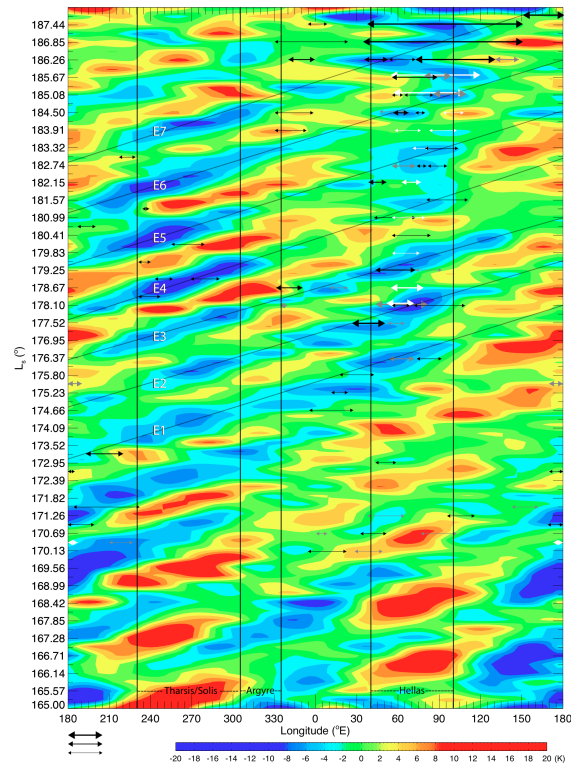


Figure 3: TES 3.7 hPa FFSM eddies at 60° S and MOC storms, MY 25

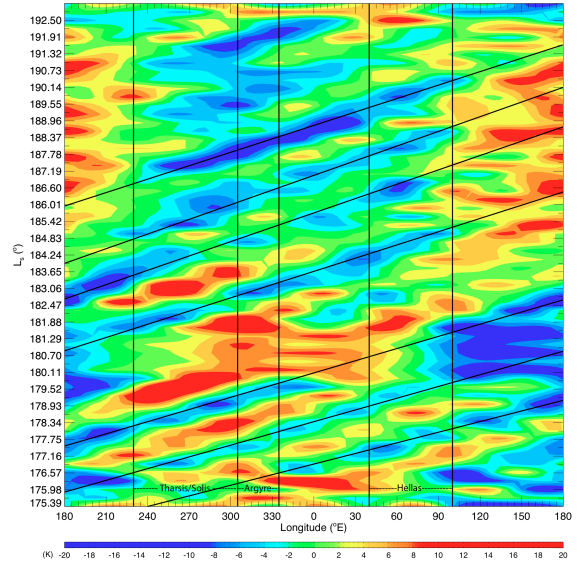


Figure 4: TES 3.7 hPa FFSM eddies at 60° S, MY 26

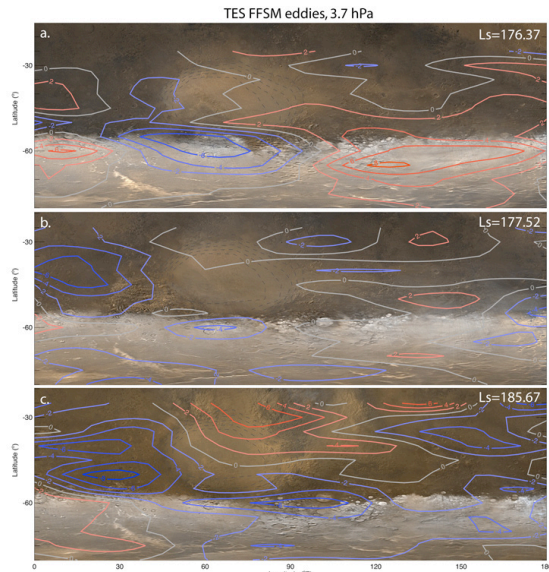


Figure 5: TES 3.7 hPa FFSM eddies (K) on MOC daily global maps, Hellas quadrant, MY 25

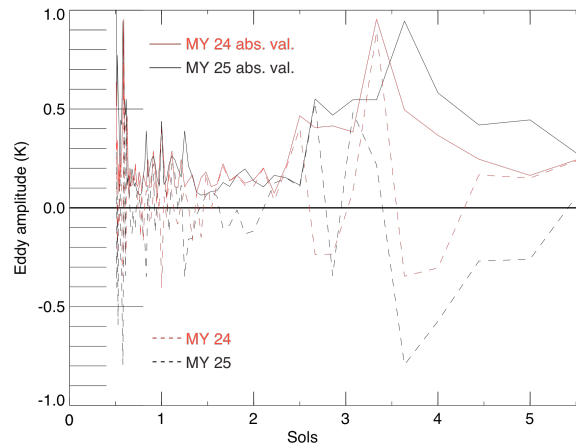


Figure 6: FFT power spectra of TES FFSM eddies in Hellas (40–100° E, 60° S) for MY 24 and 25